Hydrodynamic analysis of flagellated bacteria swimming near one and between two no-slip plane boundaries

Henry Shum*
Department of Chemical & Petroleum Engineering, University of Pittsburgh, Pittsburgh, Pennsylvania 15261, USA

Eamonn A. Gaffney†
Wolfson Centre for Mathematical Biology, Mathematical Institute, University of Oxford, Oxford OX2 6GG, United Kingdom
(Received 31 October 2014; published 20 March 2015)

The motility of swimming bacteria near solid surfaces has implications in a wide range of scenarios, including water treatment facilities, microfluidics, and biomedical implants. Using the boundary element method to numerically solve the equations of low Reynolds number fluid flow, we investigate the dynamics of a model swimmer propelled by rotating a single helical flagellum. Building on previous simulation results for swimmers near a single plane boundary, we introduce a second, parallel boundary and show that the bacterial trajectories change as the two plates are brought closer together. Analysis of this dynamical system shows that the configuration in the center of the channel and parallel to the walls is an unstable equilibrium state for large plate separations, but it becomes the only stable position for swimmers when the plate separation is reduced to three to four times the cell width. Our model also predicts that transient trajectories, i.e., those not at steady states, can exhibit curvature in the opposite sense to that expected from the well-known explanation for circular bacterial paths near a single wall.

DOI: 10.1103/PhysRevE.91.033012 PACS number(s): 47.63.Gd, 47.11.Hj, 87.17.Jj, 47.63.mf

I. INTRODUCTION

Given the prevalence of bacteria in almost every environment on Earth, it is no wonder that this diverse group of micro-organisms is involved in many of our technological achievements as well as challenges. For example, bacteria have been exploited in efforts to develop bioremediation strategies [1]. Biofilms formed by colonies of bacteria and other micro-organisms can be both beneficial, e.g., in bioreactors, and detrimental, e.g., biofouling of ship hulls, medical implants, and water filtration membranes [2,3]. These processes involve the interaction of micro-organisms with fluid-solid interfaces, and it has been observed that motility is an important factor in the initial stages of bacterial biofilm formation [4]. Hence, there is a need to develop our understanding of the effects of surfaces on the locomotion of micro-organisms.

Theoretical studies on swimming near no-slip plane boundaries date back as early as 1974 with Katz [5], where the "swimmer" was an infinite waving sheet. A more realistic, finite, model swimmer often considered consists of an inert body and a long, slender tail that propagates waves to propel the swimmer. Such models have been used for the simulation of swimming spermatozoa [6,7] and bacteria [8–10] near surfaces. From these studies, it has been found that both spermlike and bacterialike swimmers can be hydrodynamically attracted to no-slip boundaries, and, depending on the precise shape and beat pattern of the swimmer, the swimmer may tend to maintain a constant distance while swimming parallel to the wall. In particular, it was observed that swimmers with elongated bodies and short tails tend to escape from walls, whereas those with shorter, more spherical bodies and long tails are more likely to remain at walls. Similar dynamics have also been shown for "squirmers," idealized swimmers with prescribed patterns of fluid slip velocity over their bodies [11].

The hydrodynamic effects of boundaries can be qualitatively understood by examining the stress distribution that the swimmer generates in the fluid and the image system required to satisfy the no-slip boundary condition on the wall. The flow field around a swimming bacterium is well approximated by a force dipole; their tails push fluid backward and their bodies drag fluid forward as they swim [12]. The image system tends to pull the swimmer toward the wall and align the swimmer with the wall. Higher-order terms in the flow field, which depend on the swimmer's shape and method of propulsion, also contribute to the rotational and translational velocities of the swimmer and become more significant at closer distances to the wall. The overall behavior of the swimmer in the presence of boundaries is therefore approximated by the combination of these terms, as described by Spagnolie and Lauga [13].

Experimental evidence indicates that spermatozoa [14] and bacteria [15] tend to accumulate at surfaces, as predicted by hydrodynamic models. It should be noted that accumulation of swimmers at surfaces also occurs in nonhydrodynamic models relying on collisions to align swimmers with the wall [16]. However, it is likely that the hydrodynamic attraction due to the dipolar flow field prolongs the residence time once a swimmer is near the wall [12,17].

Hydrodynamic interactions are also necessary to explain another commonly observed feature of bacteria swimming near surfaces: there is a tendency for circular trajectories of a fixed handedness [17]. This is caused by the counter-rotation of the bacterial cell body and flagellum where the presence of the no-slip boundary causes a top-bottom asymmetry in resistance to motion [18]. Path curvature is sensitive to the size and shape of the swimmer; a property that has been exploited as a basis for population sorting in microfluidic channels [19].

Microfluidic devices, as well as many natural environments, pose multiple boundaries to bacteria simultaneously, so it is necessary to expand beyond analysis of a swimmer near a

*phs13@pitt.edu
†gaffney@maths.ox.ac.uk

single, planar boundary. Zöttl and Stark [20,21] investigated model microswimmers in circular tubes and between parallel plates with an imposed Poiseuille flow, giving rise to "tumbling" and "swinging" motion of the swimmers. These studies focused on the effect of the nonuniform background flow on a self-propelled particle of small size compared with the length scale of the domain confinement. Other authors have investigated cases in which the radius of the circular tube is comparable to the swimmer size [22,23] and found that trajectories in this highly confined environment depend on the type of swimmer considered. Zhu *et al.* [22] investigated squirmers and found that pushers, those with dipolar far fields of the same sign as bacteria, tended to crash into the wall, whereas pullers maintained a stable position either in the center of the tube or near the wall. Acemoglu and Yesilyurt [23] used a bacterial model swimmer and reported that the power efficiency of swimming in tubes peaked for tube diameters about 50% larger than the width of the swimmer body with typical efficiencies double those of the same swimmer in unconfined fluid. Despite such severe geometric confinement, Binz *et al.* [24] have shown experimentally that bacteria can indeed swim through channels marginally larger than their bodies, and swimming speeds in channels were found to be up to three times as high as in more open environments.

In the current work, we analyze the dynamics of a monotrichous (singly flagellated) bacterium, such as the extensively studied *Rhodobacter sphaeroides* [25,26], between two parallel no-slip plates. The boundary element method (BEM) is used to numerically solve the equations of Stokes flow to determine the motion of the model swimmer. Guided by previous results for a single plane boundary [10], we compare three swimmers differing only in the lengths of their flagella, spanning the transition from boundary-accumulating to boundary-escaping behaviors. After verifying that the dynamics between parallel plates of large separation are consistent with single wall interactions, we examine the changes to the bacterial trajectories that occur as the plate separation is reduced. We then discuss the implications that the observed hydrodynamic interactions have for bacteria in channels and other confined spaces.

II. METHODS

In this study, we employ the boundary element method to numerically solve the equations of Stokes flow for a model bacterium swimming near a single plane boundary or between two parallel plane boundaries, separated by a distance H. This process yields the instantaneous rotational and translational velocities of the bacterium for a given configuration. By considering physical symmetries of the model, we reduce the motion of the swimmer to a dynamical system in two variables: the height of the swimmer from the lower wall, h, and the inclination angle of the swimmer axis relative to the horizontal plane, θ. We then examine these reduced systems for fixed points and limit cycles.

A. Bacterial model

The model for the bacterium is identical to that used by Shum *et al.* [10]. As illustrated in Fig. 1, the swimmer

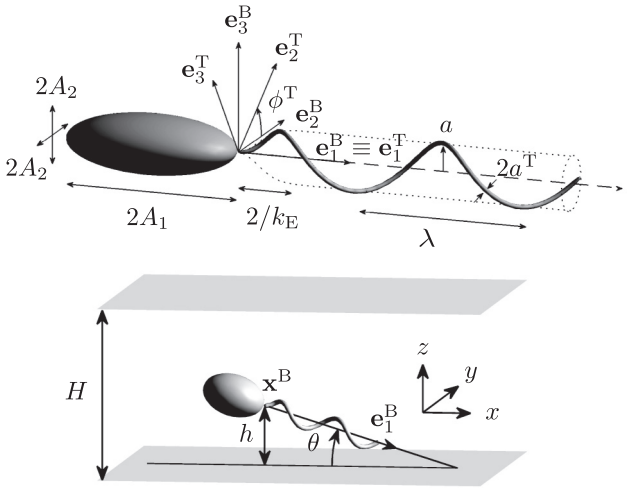

FIG. 1. Illustration of model bacterium shape (top) and configuration between parallel plates (bottom). As depicted, A_1 and A_2 are the lengths of the semimajor and -minor axes of the spheroidal cell body. The body directors $\mathbf{e}_j^{\mathrm{B}}$ and tail directors $\mathbf{e}_j^{\mathrm{T}}$ are related by a rotation through the angle ϕ^{T} about the $\mathbf{e}_1^{\mathrm{B}}$ axis. The flagellum has a cross-sectional radius a^{T} and grows into a helix of amplitude a and wavelength λ. The total length of the flagellum is L, measured along the curved centreline. The position of the bacterium relative to a fixed reference frame is described by the vector $\mathbf{x}^{\mathrm{B}}$. For swimming in the presence of plane boundaries, we track the distance from the wall below, h, and the angle of inclination, θ. Between parallel plates, the plate separation is H.

consists of two neutrally buoyant rigid structures: a spheroid representing the cell body and a thin filament of helical shape with an amplitude envelope as suggested by Higdon [27] so that the flagellum emerges from the cell body at a point on the axis of the helix. We fix the parameter $k_{\mathrm{E}} = 2\pi/\lambda$ so that the helical amplitude grows to its full value over a distance $2/k_{\mathrm{E}} \sim \lambda/3$. Lengths in our model are nondimensionalized by the volumetric radius of the spheroidal cell body, $\bar{a} = (A_1 A_2^2)^{1/3}$. For the well-studied monotrichous bacterium, *R. sphaeroides*, one finds $\bar{a} \approx 0.5\ \mu$m [25]. This bacterium has a flagellar length in the range 1–6 μm [26]. Nonetheless, below we restrict our study to flagellar lengths of $5\bar{a}$–$7.5\bar{a}$, corresponding to 3.5–5.25 μm.

We also note that these flagellar lengths are roughly consistent with, but slightly lower than, those of the most commonly studied bacterium, *Escherichia coli*, which has flagella of length 7–10 μm [28,29]. However, *E. coli* is peritrichous (multiflagellated) and hence its flagella wrap around the cell body before forming a flagellar bundle that emerges from the pole of the cell body. This means that the length of the flagellar bundle projecting from the cell pole is significantly shorter than the length of the individual flagella.

We allow a small gap of size $\bar{a}/10$ (of the order of a flagellum radius) between the body and the flagellum to avoid constructing an ill-posed problem with singular velocity gradients due to the relative motion of the two structures [8].

The reference point of the bacterium is taken to be the pole of the cell nearer the flagellum, and it will be referred to as the swimmer position, denoted $\mathbf{x}^{\mathrm{B}}$. The instantaneous configuration of the swimmer is fully described by the

swimmer position, the body directors $\mathbf{e}_j^{\mathrm{B}}$, and the tail phase ϕ^{T}, which describes the rotation about the axis $\mathbf{e}_1^{\mathrm{B}}$ from the body directors to the tail directors. The motion of the bacterium can therefore be described by a translational velocity $\mathbf{U}$, a rotational velocity $\mathbf{\Omega}$, and a motor speed ω^{M}, according to the relations

$$\frac{d}{dt}\mathbf{x}^{\mathrm{B}} = \mathbf{U}, \quad \frac{d}{dt}\mathbf{e}_j^{\mathrm{B}} = \mathbf{\Omega} \times \mathbf{e}_j^{\mathrm{B}}, \quad \frac{d}{dt}\phi^{\mathrm{T}} = \omega^{\mathrm{M}}. \tag{1}$$

The two structures themselves remain rigid during motion. Writing the relative position of a point as $\tilde{\mathbf{x}} = \mathbf{x} - \mathbf{x}^{\mathrm{B}}$, the velocity at a point on the surface of the swimmer can be expressed as

$$\mathbf{u}(\mathbf{x}) = \begin{cases} \mathbf{U} + \mathbf{\Omega} \times \tilde{\mathbf{x}}, & \mathbf{x} \in B, \\ \mathbf{U} + \left(\mathbf{\Omega} + \omega^{\mathrm{M}}\mathbf{e}_1^{\mathrm{B}}\right) \times \tilde{\mathbf{x}}, & \mathbf{x} \in T, \end{cases} \tag{2}$$

where B denotes the surface of the cell body and T denotes the surface of the flagellum.

B. Solving instantaneous dynamics

The fluid around the swimmer is governed by the equations of unforced, incompressible Stokes flow,

$$-\nabla p + \mu\nabla^2\mathbf{u} = \nabla \cdot \boldsymbol{\sigma} = \mathbf{0}, \quad \nabla \cdot \mathbf{u} = 0, \tag{3}$$

where p is the pressure, μ is the dynamic viscosity, $\mathbf{u}$ is the velocity field, and $\boldsymbol{\sigma}$ is the Cauchy stress tensor field.

The solution to these equations can be expressed as a boundary integral equation; in the single-layer potential formulation [30],

$$u_j(\mathbf{X}) = -\int_{\partial V} f_i(\mathbf{x}) G_{ij}(\mathbf{x},\mathbf{X}) dS(\mathbf{x}), \tag{4}$$

where $\mathbf{f}$ is the traction vector field acting over the boundary enclosing the fluid domain, ∂V, and G_{ij} are the ij components of the Stokeslet Green's function defined by

$$G_{ij}(\mathbf{x},\mathbf{X}) = \frac{1}{8\pi\mu}\left(\frac{\delta_{ij}}{R} + \frac{R_i R_j}{R^3}\right), \tag{5}$$

where $\mathbf{R} := \mathbf{x} - \mathbf{X}$ and $R := \|\mathbf{R}\|$. The boundary of the fluid consists of four parts, $\partial V = B \cup T \cup W \cup \partial V_\infty$, where B and T are the surfaces of the cell body flagellum, respectively, W is the collection of confining plane boundaries, and ∂V_∞ denotes the surface at infinity. Since the velocities and traction are assumed to vanish at infinity, we can neglect the ∂V_∞ portion of the boundary.

The no-slip boundary conditions require the surface velocity distributions on the swimmer given by Eq. (2), supplemented with the condition on the plane walls: $\mathbf{u}(\mathbf{x}) = \mathbf{0}, \mathbf{x} \in W$. The translational and rotational velocities $\mathbf{U}$ and $\mathbf{\Omega}$ are unknowns to be determined through additional constraints, while ω^{M} is a prescribed, constant motor speed.

Note that the absence of inertia in the Stokes flow equations and a brief consideration of dimensions entail that this motor speed simply sets the time scale of the dynamics. In particular, over any given time interval, the net displacement of the swimmer is determined by the angular displacement $\Delta\phi^{\mathrm{T}}$ of the flagellum during this interval, and hence the shape of the trajectory traced out by the swimmer is independent of any fluctuations in the motor speed. Prescribing a constant motor torque (or any other specification of how the motor operates) rather than a constant motor speed would yield the same trajectory except for a possible change in the time variable. As we do not address issues of swimming speed, we do not need to incorporate how the viscosity, temperature, drag, and biophysical limitations impact the bacterial motor rotation, constituting a significant, though fully justified, simplification of the bacterial model.

We further assume that the swimmer is neutrally buoyant and therefore experiences no net force or torque, requiring the conditions

$$\int_{B\cup T} \mathbf{f} dS = \mathbf{0}, \quad \int_{B\cup T} \tilde{\mathbf{x}} \times \mathbf{f} dS = \mathbf{0}. \tag{6}$$

We discretize the boundaries with a mesh of quadratically interpolated triangular elements as previously described [10]. A typical simulation uses a mesh with ~400 nodes on the flagellum and ~250 nodes on the cell body. For each wall, we mesh a finite section of the plane near the swimmer, $|x_j - x_j^{\mathrm{B}}| < 50\bar{a}$, for components parallel to the wall, $j = 1,2$. Approximately 400 nodes are distributed over each wall mesh, with a higher density close to the swimmer. Using the boundary element method, we approximate boundary integrals with quadrature over the mesh and solve Eq. (4) together with the constraints (6) to obtain the traction distribution $\mathbf{f}$ over the bacterial body, flagellum, and plane boundaries, as well as the kinematic quantities $\mathbf{U}$ and $\mathbf{\Omega}$ describing the motion of the bacterium.

C. Phase-averaged dynamical system

We reduce the dimensionality of the bacterial dynamics by taking advantage of the symmetry properties of the swimmer and of the fluid domain. We first average the dynamics over one revolution of the motor with the cell body held fixed [31]. Results of previous studies of the bacterial swimmer [31] indicate that more than 10 motor revolutions are needed to propel the organism forward a distance of one helical wavelength. Therefore, it is reasonable to consider the swimmer position fixed on the time scale of a motor revolution. Some precession of the cell orientation will also occur, but this is small [32]. By axisymmetry of the spheroidal cell body, the dynamics are independent of the transverse directors, $\mathbf{e}_2^{\mathrm{B}}$ and $\mathbf{e}_3^{\mathrm{B}}$. The mean velocity is therefore written as

$$\begin{aligned} \bar{\mathbf{U}}\left(\mathbf{x}^{\mathrm{B}},\mathbf{e}_1^{\mathrm{B}}\right) &= \frac{1}{2\pi}\int_0^{2\pi} \mathbf{U}\left(\mathbf{x}^{\mathrm{B}},\mathbf{e}_j^{\mathrm{B}},\phi^{\mathrm{T}}\right) d\phi^{\mathrm{T}} \\ &\approx \frac{1}{N_\phi}\sum_{k=1}^{N_\phi} \mathbf{U}\left(\mathbf{x}^{\mathrm{B}},\mathbf{e}_j^{\mathrm{B}},\phi^{\mathrm{T}} = \frac{2\pi k}{N_\phi}\right), \end{aligned} \tag{7}$$

where $\mathbf{U}(\mathbf{x}^{\mathrm{B}},\mathbf{e}_j^{\mathrm{B}},\phi^{\mathrm{T}})$ denotes the velocity computed for the swimmer using the BEM with position $\mathbf{x}^{\mathrm{B}}$, orientation vectors $\mathbf{e}_j^{\mathrm{B}}$, $j = 1,2,3$, and motor phase ϕ^{T}. The mean cell body rotation rate, $\bar{\mathbf{\Omega}}$, is defined analogously. The specification of directors $\mathbf{e}_2^{\mathrm{B}}$ and $\mathbf{e}_3^{\mathrm{B}}$ is arbitrary, as any dependence on these is solely due to discretization and numerical errors. For the results presented herein, we adaptively use $N_\phi = 8$, 16, or 32, depending on the rate of convergence of the computed mean.

Consider the bacterium near an infinite plane boundary or between two parallel planes with normal in the z direction. By symmetry, the dynamics of the swimmer must be invariant to translations parallel to the wall. In addition, rotating the bacterium about the direction perpendicular to the wall is equivalent to a rotation of the coordinate frame. If we place the swimmer as shown in Fig. 1 so that the bacterial axis $\mathbf{e}_1^{\mathrm{B}}$ lies in the x-z plane, then the mean velocities are determined by the height $h \equiv x_3^{\mathrm{B}}$ and inclination angle $\theta = -\arcsin(\hat{\mathbf{z}} \cdot \mathbf{e}_1^{\mathrm{B}})$, where $\hat{\mathbf{z}}$ is the unit normal to the plane surfaces, pointing away from the lower plane. The rates of change of these variables are given by

$$\begin{aligned} \dot{\theta}(\theta,h) &= \bar{\Omega}_2(\theta,h), \\ \dot{h}(\theta,h) &= \bar{U}_3(\theta,h). \end{aligned} \tag{8}$$

We follow the scheme employed by Shum *et al.* [10] to efficiently compute trajectories of swimmers from many initial conditions using averaged dynamics. We first generate a look-up table of mean translational and rotational velocities on a grid of (θ,h) values. The functions $\bar{\Omega}_2(\theta,h)$ and $\bar{U}_3(\theta,h)$ in Eq. (8) are approximated using linear interpolation with the preevaluated data points and used to solve the two-dimensional ODE system for $\theta(t)$ and $h(t)$.

III. RESULTS

A. One plane boundary

We classify swimmer behavior as either boundary-accumulating or boundary-escaping. Boundary accumulators are swimmers that tend to remain close to walls due to a hydrodynamic influence. They exhibit a stable swimming configuration relative to the wall and move parallel to the wall with some steady inclination angle. To avoid the issue of direct cell-surface interactions, which depend on many factors (see, e.g., Klein *et al.* [33]), we do not consider boundary accumulators that have a tendency to collide with walls. In our phase plane analyses, we do not include dynamics for configurations in which any part of the swimmer is less than $d_{\min} = 0.05\bar{a}$ from the wall; we treat these as "collisions" with the wall.

Boundary escapers are hydrodynamically repelled by walls; given any starting position and orientation, the swimmer will have a finite residence time at the wall before moving away. Evidence suggests that hydrodynamic interactions with walls have little effect on bacterial motion beyond a distance of about one cell length [12]. For the purposes of this study, we consider a swimmer to have escaped from the wall when the cell body–flagellum junction reaches a height $h/\bar{a} = 10$, roughly one swimmer length including the flagellum. Increasing the threshold used in this definition would not qualitatively affect our conclusions.

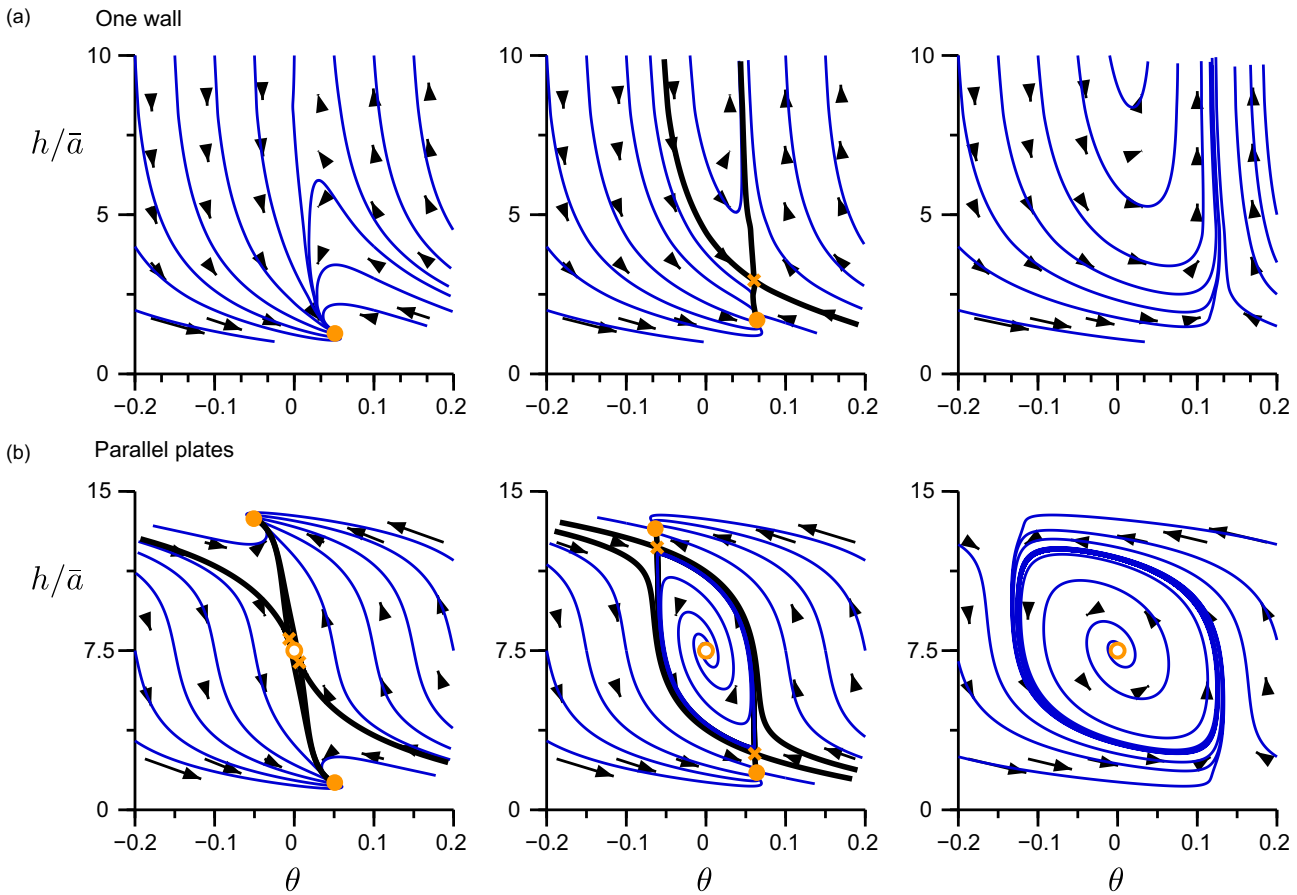

FIG. 2. (Color online) Phase plane diagrams for bacteria swimming (a) near a single no-slip plane boundary and (b) between parallel plates with plate separation $H/\bar{a} = 15$. Flagellar lengths are (left column) $L/\bar{a} = 7.5$, (center column) $L/\bar{a} = 6.5$, and (right column) $L/\bar{a} = 5$. Stable fixed points are indicated by filled circles, unstable fixed points at $(\theta = 0, h/\bar{a} = 0)$ are indicated by open circles, and saddle nodes are indicated by crosses (×). Trajectories entering and leaving saddle nodes are shown with thicker curves.

It is known from previous simulation studies that the trajectories of individual flagellated bacteria near no-slip surfaces are strongly influenced by the shape and size of the cell body and helical flagellum [9,10,34]. Some combinations of parameters give rise to boundary accumulators, while others produce boundary escapers. We choose to focus on one parameter to vary in this study: the flagellar length, L. A transition was shown to occur from boundary escape for small L to boundary accumulation for large L [10].

In Fig. 2(a), we illustrate this bifurcation in (θ,h) phase-space behavior as the flagellum length is reduced from $L = 7.5\bar{a}$ to $5\bar{a}$. Other geometrical parameters are fixed at the values $\lambda = 1.8\bar{a}$, $A_1/A_2 = 3$, $a = \lambda/2\pi$, $a^{\mathrm{T}}/\bar{a} = 0.05$. Starting with the longest flagellum length, $L/\bar{a} = 7.5$, we find a stable state near the wall with a large basin of attraction. Bacteria that are initially inclined sharply away from the wall will escape, and those sharply inclined toward the wall collide with the wall. Apart from these extreme initial conditions, the swimmer will reach the stable state. From the phase plane diagram, we expect that instantaneous perturbations from the steady state as large as $4\bar{a}$ vertically would decay.

Decreasing the flagellum length reveals a new regime in which approaching swimmers are attracted and remain close to the boundary only if the angle of incidence is sharp enough. Shallow approaches are deflected away and the cell escapes from boundary effects. In this case, a vertical perturbation of $1.5\bar{a}$ from the steady state is sufficient to cause the swimmer to escape from the surface. If the flagellum length is decreased further, the stable state is lost and all approaching trajectories are deflected back into the bulk fluid.

B. Parallel plane boundaries

We would expect the behavior of a bacterium swimming near a single no-slip plane boundary to be similar to the case between parallel plates if the gap is sufficiently large. For comparison, we present the phase plane diagrams for a plate separation $H/\bar{a} = 15$ in Fig. 2(b) below the diagrams for the same swimmers near a single wall [Fig. 2(a)]. Near each plate, we observe the same transition from accumulating to escaping as the flagellum length decreases. If the flagellum is long enough, regardless of initial conditions, the swimmer is attracted to the stable point at one of the planes. By symmetry, the configuration parallel to and exactly halfway between the plates is also a fixed point $(\theta = 0,h = 0)$. This was found to be an unstable spiral point. With short flagella, a bacterium approaching a wall is deflected away. However, between parallel planes, this swimmer will approach the opposite wall. It is repeatedly deflected and continually bounces from one wall to the other. This is manifest in a limit cycle in the phase plane. Under these conditions, the central fixed point, $(\theta = 0,h = 0)$, was again found to be unstable and the limit cycle was stable. Hence, all trajectories approach the limit cycle and swimmers are all expected to exhibit this behavior. In the intermediary case, for which both attractive and repulsive regions were found near a single wall, trajectories approach either a limit cycle or a stable point near one of the walls.

As the plate separation is decreased, both walls become simultaneously influential to the swimming dynamics, and we can no longer consider the bacterium to be simply interacting with one wall at a time. With a plate separation $H/\bar{a} = 10$ [Figs. 3(a) and 3(b)], the phase plane diagrams are qualitatively

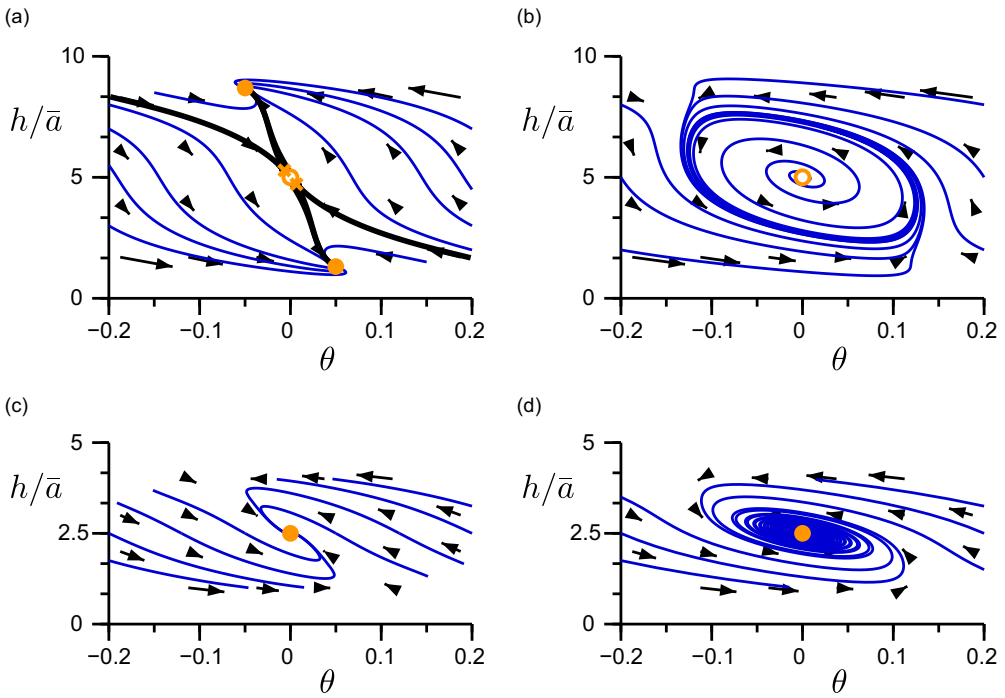

FIG. 3. (Color online) Phase plane diagrams for bacteria between parallel plates. Flagellar lengths are (left column) $L/\bar{a} = 7.5$ and (right column) $L/\bar{a} = 5$. Plate separations are (top row) $H/\bar{a} = 10$ and (bottom row) $H/\bar{a} = 5$. The boundary accumulator $(L/\bar{a} = 7.5)$ is attracted to a stable state at the walls when the plate separation is large but is attracted to the center of the channel when the separation is small. The boundary escaper $(L/\bar{a} = 5)$ oscillates between walls when the plate separation is large but converges to the center when the separation is small.

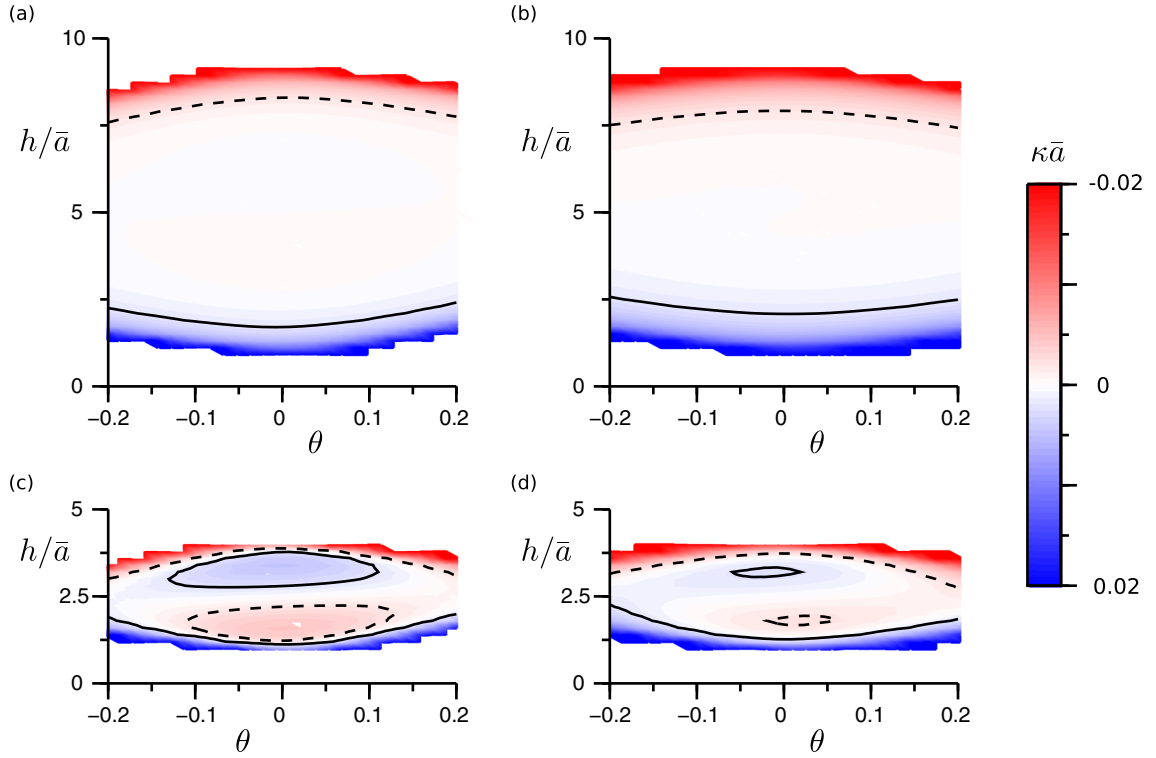

FIG. 4. (Color online) Instantaneous curvature (κ) maps for x-y projection of the bacterial path between parallel plates. (a) Boundary accumulator in a channel of height $H/\bar{a} = 10$. (b) Boundary escaper in a channel of height $H/\bar{a} = 10$. (c) Boundary accumulator in a channel of height $H/\bar{a} = 5$. (d) Boundary escaper in a channel of height $H/\bar{a} = 5$. Contour curves roughly separate low from high magnitudes of curvature, with threshold $|\kappa\bar{a}| = 0.002$. Dashed curves are used for negative curvature (clockwise circles viewed from above) and solid curves are used for positive curvature (counterclockwise). Unshaded regions near $h = 0$ and $h = H$ are unreachable due to intersection or close proximity ($d_{\min} = 0.05\bar{a}$) of the wall and swimmer.

the same as with the larger separation $H/\bar{a} = 15$. Further decreasing the plate separation to $H/\bar{a} = 5$, however, we find that a bifurcation occurs, leading to qualitatively different trajectories. In the case of boundary accumulators, the stable fixed points at the walls disappear [Fig. 3(c)], and for boundary escapers, the limit cycle disappears [Fig. 3(d)]. For both types of swimmers, the central fixed point becomes stable at small plate separations. Hence, both boundary accumulators and escapers tend to swim in the center of thin channels.

C. Path curvature

Having described the tendencies of swimmers to move away from and toward walls, we now examine the motion in the plane parallel to the walls. Using the phase-averaged translational and rotational velocities, we compute the curvature of the x-y projection of the swimmer's path as

$$\kappa = \frac{\bar{\Omega}_3 + \bar{\Omega}_1 \tan(\theta)}{\sqrt{\bar{U}_1^2 + \bar{U}_2^2}}. \tag{9}$$

This kinematic formula is consistent with the expression for the radius of curvature used by Shum *et al.* [10], where it was assumed that the steady state was reached so that translational motion was purely in the x-y plane. Since angular and translational velocities depend on $h/\bar{a}$ and θ, so does the path curvature. The observed curvature for a given bacterium will therefore vary with time unless the swimmer is in a stable configuration. The dependence of the instantaneous path curvature on position and inclination is shown in Fig. 4, where regions of appreciable curvature are indicated by contours at $|\kappa\bar{a}| = 0.002$. For comparison, *E. coli* cells have been observed to swim in circles of radius $R \sim 25$ μm at walls [35], corresponding to $\kappa\bar{a} \sim 0.02$.

For large plate separations, there is a thin region near each wall where the curvature is high, but for most of the space between the two plates, the curvature magnitude is less than $0.002/\bar{a}$. Little difference can be seen between the boundary accumulator and the boundary escaper. Note that the sign of the curvature changes roughly midway between the plates. That is, the direction of curvature only depends on which wall the swimmer is closer to. This is not the case, however, when the plate separation is small [$H/\bar{a} = 5$, Figs. 4(c) and 4(d)]. When the swimmer is at distances of around $0.2\bar{a}$ from collision with a wall, the sign of the path curvature is still consistent with the larger plate separation case. For swimmers farther from the wall, we find that over a wide range of $h/\bar{a}$ and θ, the sign of the curvature is reversed and the swimmer turns in the sense expected from interaction with the opposite wall. The magnitude of curvature in these "anomalous" zones reaches a maximum of approximately $0.005/\bar{a}$. As with the larger plate separation, there was no qualitative difference between the boundary accumulator and the boundary escaper

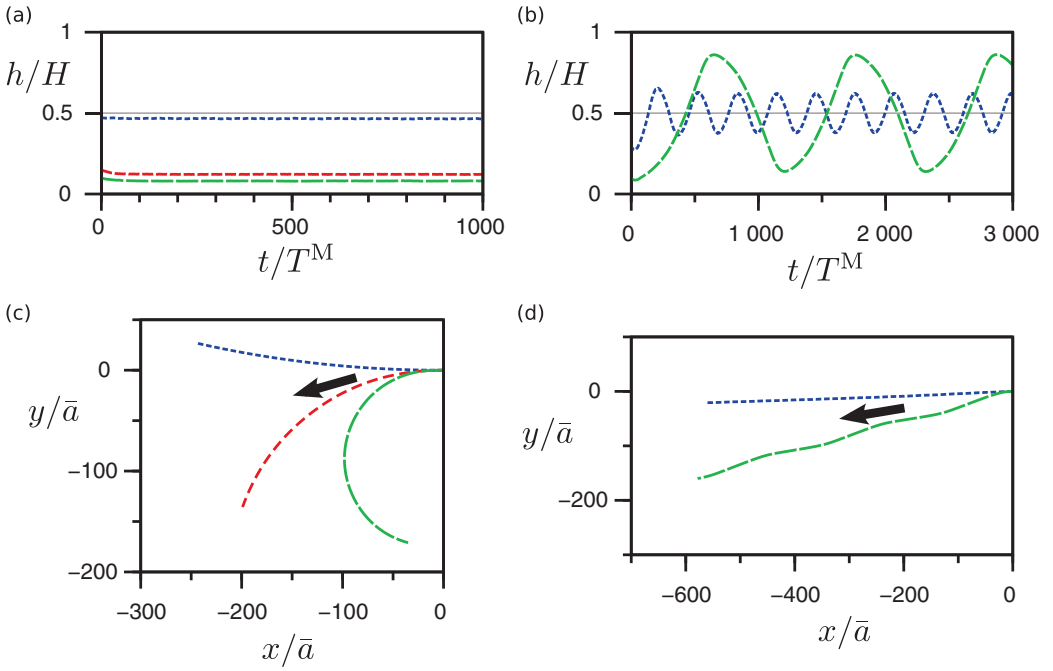

FIG. 5. (Color online) Trajectories of model bacteria using simulations of full dynamics. Oscillations on the time scale of a motor revolution are too small to be visible in these plots. (a) Time series of height from the wall for boundary-accumulating swimmers starting close to respective steady states predicted by phase-averaged dynamics in channels of height $H/\bar{a} = 5$ (short-dashed line), $H/\bar{a} = 10$ (medium-dashed line), and $H/\bar{a} = 15$ (long-dashed line). The time scale, $T^{\mathrm{M}} = 2\pi/\omega^{\mathrm{M}}$, is the motor period. (b) Time series of height from the wall for boundary escapers in channels of height $H/\bar{a} = 5$ (short-dashed line) and $H/\bar{a} = 15$ (long-dashed line). (c),(d) Top-down views of trajectories from (a) and (b), respectively, with arrows indicating the direction of motion. Note that although all boundary accumulators were closer to the lower wall than to the upper wall, the path in the channel of height $H/\bar{a} = 5$ curved in the opposite direction from those in larger channels.

in terms of the instantaneous path curvature, though the anomalous curvature was more significant with the boundary-accumulating swimmer shape.

D. Trajectory simulations with full dynamics

To verify the results of the flagellum phase-averaged dynamical model in the preceding sections, we perform time-stepping simulations of the full system, resolving the variations in velocities over each revolution of the flagellum. Examples of trajectories for boundary accumulators and escapers are shown in Fig. 5. For the larger plate separations, $H/\bar{a} = 15$ and 10, the boundary behavior agrees with the phase-averaged predictions; the boundary accumulator remains close to the wall and the boundary escaper oscillates between walls [Figs. 5(a) and 5(b)]. In the case of the smallest plate gap size, $H/\bar{a} = 5$, the swimmers were predicted to converge to the center of the gap. In the full simulation, the boundary-accumulating bacterium maintained a slight distance from the center of the narrowest channel, while the boundary-escaping swimmer maintained oscillations, though with reduced amplitude, about the center of the channel. These small discrepancies appear to be due to approximations in phase-averaging. The top-down view of the trajectories reveals the effects of plate separation on path curvature [Figs. 5(c) and 5(d)]. Reducing the separation from $H/\bar{a} = 15$ to 10 leads to a lesser counterclockwise curvature in the path of the boundary accumulator despite the stable distance from the wall being approximately the same. With the narrowest plate separation, we observe a path that curves in the clockwise direction. This is in agreement with our phase-averaged model predictions for a swimmer slightly displaced from the center when the plate separation is small.

For boundary-escaping swimmers between plates of both wide and narrow separation, the observed path curvatures are much smaller in magnitude than for boundary accumulators, and they alternate in sign, leading to long-ranged directed transport rather than circular orbits. With large plate separations, alternating slight left and right turns can be seen, corresponding to the escaper "bouncing" off the bottom and top wall, respectively [Figs. 5(b) and 5(d)].

IV. DISCUSSION

As has previously been demonstrated, the motion of a bacterium-like microswimmer near boundaries was found to be dependent on the details of the swimmer shape. In this study, we varied the flagellum length, with the longest increased by 50% compared to the shortest. This difference was sufficient to change the behavior from boundary-accumulating to boundary-escaping. Hence, we can expect that in a population of bacteria with variable sizes and ages, there could be some individuals that tend to swim near boundaries and others that tend to avoid boundaries. Furthermore, stochastic fluctuations in the motor actuation, along with Brownian rotation of the bacterium, could cause boundary accumulators to escape from surfaces.

Between parallel plates, our model predicts three classes of long-term behavior: (i) circular orbiting close to one wall, (ii) straight trajectories parallel to and midway between walls,

and (iii) "bouncing" repeatedly from wall to wall. The class that is observed depends on both the swimmer shape and the wall separation. For this purpose, we distinguish swimmer shapes only by whether the swimmer tends to swim close to a single no-slip plane boundary (boundary accumulating) or escapes (boundary escaping). Circular orbits are predicted to occur for boundary-accumulating bacteria when the gap between the walls is large compared with the swimmer size. This mode is commonly observed experimentally with most motile bacteria swimming at a solid surface.

When the gap is sufficiently small, of the order of one body length, the trajectory becomes a straight line parallel to and midway between the walls. This switch in behavior has important consequences in both natural and artificial situations. For example, swimming in a straight line in a confined space would allow the organism to explore space and escape into a more open environment. We can also infer that bacteria may have a tendency to become trapped and accumulate on the walls of large chambers while passing directly through channels of shallow depth. Thus, channel depth is an important consideration for the control of bacterial migration through microfluidic systems.

We remark that the stable state midway between close plates is further from the walls than the stable state close to widely separated plates. This, combined with the entrapment of bacteria in circular orbits at a single wall, suggests the somewhat counterintuitive possibility that bacteria without a predisposition to surface collision are less likely to adhere to a surface when they are strongly confined between two closely separated plates than when the plates are farther apart. If this prediction is correct, it could be possible to reduce bacterial colonization of tubes and channels, in constructs such as prospective microdevices, by dividing the structure into multiple parallel thin channels or narrow tubes. However, narrow passageways are likely to be more susceptible to blockage and require greater pressure gradients to maintain a given flux. Details of bacterial attachment processes are important, necessitating experiments and simulations for further exploration of this issue.

A recent study by Swiecicki *et al.* [36] gives experimental evidence for the behavior of peritrichous (multiflagellated) bacteria, *E. coli*, between parallel plates of varying separations. Regular planktonic cells (length $\sim 2\ \mu$m) were found to swim in circles in channels of height greater than $3\ \mu$m, corresponding to the boundary-accumulating state. Decreasing the separation between the top and bottom walls to $2.5\ \mu$m or less, the bacteria were found to swim in figure-8 patterns, which the authors explained as crossing an energy barrier from a bound state at one wall to a bound state at the other wall, which would give rise to circular orbits in opposite directions. The frequency of crossing between clockwise and counterclockwise orbits increased as the channel height was reduced. In narrow channels (height $< 2.5\ \mu$m), straight trajectories were observed, though only in artificially elongated cells of length $\sim 6\ \mu$m. It was hypothesized that for these swimmers, the hydrodynamic interaction potentials from the two walls merged to form a single energetic minimum midway between the walls, causing cells to swim in the middle with little path curvature. Our hydrodynamic analysis confirms that this can, indeed, occur for boundary accumulators between closely separated plates. The fact that linear trajectories were only observed for elongated cells could be due to the weaker boundary accumulation of high aspect ratio swimmers [10] allowing the central configuration to be stable at larger plate separations. Furthermore, elongated cells, which maintain the same width, have larger volume and therefore are subject to more extensive hydrodynamic interactions and thus confinement compared to shorter cells in the same channel.

It should be noted that such comparisons are subject to the caveat that our model assumes a single flagellum at the pole of the cell whereas *E. coli* have many flagella that wrap around and form a bundle behind the cell. This could result in a difference in dynamics. It has been shown that boundary-accumulating behavior in monotrichous swimmers is sensitive to the bending stiffness of the hook connecting the bacterial motor to the flagellum [37]. With multiple flagella forming a bundle in peritrichous bacteria, elastic effects are fundamental and will also, most likely, play a role in determining the swimming behavior near boundaries, although the extent of this role is unexplored.

A somewhat surprising prediction from our model is the emergence, in channels of small plate separation, of regions roughly $1/4$ of the channel height from each wall in which the bacteria curve in the direction associated with swimming near the opposite wall. The magnitude of curvature in these regions increases for smaller plate separations but remains less than that of swimmers very close to the wall. Nonetheless, this effect means that the curvature is more sensitive to height variations when there is close confinement by a second wall. A bacterium can switch between clockwise and counterclockwise arcs due to small changes in height without necessarily crossing from one wall to the other.

The reversed curvature can be explained by considering the motion of objects between parallel no-slip boundaries. Ganatos *et al.* [38] showed that a sphere rotating without translation about an axis parallel to the walls would experience a lateral force that could change in sign by varying the plate separation while keeping the position of the sphere relative to the closer wall fixed. For simplicity, suppose that the bacterium cell body and flagellum behave as counter-rotating spheres. The lateral forces on the body and flagellum act in opposite directions, resulting in a torque that rotates the swimmer about the wall normal direction, as described in greater detail by Lauga *et al.* for bacteria near a single plane boundary [18]. The presence of the second no-slip wall can reverse the directions of the forces on the body and flagellum, depending on the position of the swimmer and the channel height, resulting in the reversed curvature we observe.

Boundary-escaping swimmers generally follow paths of much lower curvature since they avoid the rotation-inducing boundaries. These swimmers exhibit the third form of motion we observe: "bouncing" between the top and bottom plates in nearly straight trajectories. Oscillations are suppressed by confinement, but for large plate separations, the inclination angle will tend to oscillate between 0.1 rad, or 6°, above and below the horizontal.

This angle of 0.1 rad also appears as the dominant scattering angle for boundary escapers leaving a single plane boundary. The phase plane diagram for $L/\bar{a} = 5$ in Fig. 2(a) shows a "funneling" of trajectories toward this inclination angle as the

swimmers deflect and escape from the wall. This effect is particularly significant if we consider swimmers that collide with the wall at sharper angles than included in the phase plane diagram (i.e., $\theta < -0.2$) and align with the wall due to steric interactions. Provided collisions do not result in attachment to the surface, we would expect the bacterium to swim away from the wall with an outgoing angle of roughly 6° irrespective of the incoming angle. This finding is reminiscent of experimental observations of the alga, *Chlamydomonas reinhardtii*, by Kantsler *et al.* [39]. For these micro-organisms, the constant scattering angle was determined to be due to contact between the waving flagella and the wall. Our analysis of model bacteria does not include direct contact with walls, but an analogous outcome emerges from hydrodynamic interactions.

V. CONCLUSION

By analyzing the phase plane diagrams for the dynamics of bacterium-like model swimmers near a single no-slip boundary and between two parallel plates, we have shown that qualitatively different trajectories can arise depending on the swimmer and the plate separation.

When the gap between parallel plates is greater than about one or two swimmer lengths (∼10 μm for typical bacteria), the swimmer effectively interacts with one wall at a time and the behavior can be inferred from previously known results for single plane boundaries [10]; swimmers either tend to collide with walls, migrate to a stable configuration swimming parallel and close to the wall, or escape from the wall due to hydrodynamic interactions. We found a tendency for boundary-escaping swimmers to leave the wall with a particular angle, about 0.1 radians for the swimmer shape used here. Between parallel plates, boundary-escaping swimmers are repeatedly deflected from one wall to the other in nearly linear trajectories. Boundary-accumulating swimmers are invariably attracted to stable circular orbits near one of the walls. Swimmers with intermediate shapes can exhibit both types of behavior. If such swimmers are subjected to stochastic fluctuations, as physical bacteria are, we could expect alternating periods of "bouncing" between walls and tracing out circular arcs along the walls.

Reducing the plate separation leads to a change in behavior for both boundary-accumulating and -escaping swimmers. When the plates are strongly confining, both types of swimmers are attracted to the center of the channel, swimming parallel to the walls. This is particularly significant for boundary-accumulating swimmers because it implies a transition from circular orbits to linear trajectories, which allow quick migration of the organisms. A suitably chosen plate separation could potentially be used to fractionate a population of bacteria by allowing only individuals of a certain characteristic to pass through freely.

We also found an intriguing theoretical prediction of curvature reversal; a swimmer moving parallel to the walls roughly midway between a wall and the center of the channel should follow a curved path of opposite curvature to that when the swimmer is very close to the wall.

Recent experimental evidence is consistent with our predictions for the transition from curved to straight paths of boundary accumulators in channels of decreasing height [36]. Other outcomes of our theoretical analyses can also be verified experimentally with currently available techniques. For example, bacterial flagella can be sheared and allowed to grow back [29]. At different stages of regrowth, we would be able to observe bacteria with flagella of different lengths and monitor boundary-accumulating behavior. Further experimental studies, guided by theoretical predictions, would help us to better understand and control the locomotion of bacteria in confined environments. Similar remarks apply for prospective future modeling studies, to understand the impact of biodiversity by further exploring parameter space, the role of the bacterial hook compliance, and flagellar bundling in swimming dynamics for bacteria in confined geometries together with a more extensive investigation of different geometries and surface topographies.

[1] D. H. Pieper and W. Reineke, Engineering bacteria for bioremediation, Curr. Opin. Biotech. **11**, 262 (2000).

[2] T. Leiknes and H. Ødegaard, The development of a biofilm membrane bioreactor, Desalination **202**, 135 (2007).

[3] H.-C. Flemming, Biofouling in water systems — cases, causes and countermeasures, Appl. Microbiol. Biotechnol. **59**, 629 (2002).

[4] G. O'Toole, H. B. Kaplan, and R. Kolter, Biofilm formation as microbial development, Ann. Rev. Microbiol. **54**, 49 (2000).

[5] D. F. Katz, On the propulsion of micro-organisms near solid boundaries, J. Fluid Mech. **64**, 33 (1974).

[6] D. J. Smith, E. A. Gaffney, J. R. Blake, and J. C. Kirkman-Brown, Human sperm accumulation near surfaces: A simulation study, J. Fluid Mech. **621**, 289 (2009).

[7] K. Ishimoto and E. A. Gaffney, A study of spermatozoan swimming stability near a surface, J. Theor. Biol. **360**, 187 (2014).

[8] M. Ramia, D. L. Tullock, and N. Phan-Thien, The role of hydrodynamic interaction in the locomotion of microorganisms, Biophys. J. **65**, 755 (1993).

[9] D. Giacché, T. Ishikawa, and T. Yamaguchi, Hydrodynamic entrapment of bacteria swimming near a solid surface, Phys. Rev. E **82**, 056309 (2010).

[10] H. Shum, E. A. Gaffney, and D. J. Smith, Modelling bacterial behaviour close to a no-slip plane boundary: The influence of bacterial geometry, Proc. R. Soc. A **466**, 1725 (2010).

[11] K. Ishimoto and E. A. Gaffney, Squirmer dynamics near a boundary, Phys. Rev. E **88**, 062702 (2013).

[12] K. Drescher, J. Dunkel, L. H. Cisneros, S. Ganguly, and R. E. Goldstein, Fluid dynamics and noise in bacterial cell–cell and cell–surface scattering, Proc. Natl. Acad. Sci. (USA) **108**, 10940 (2011).

[13] S. E. Spagnolie and E. Lauga, Hydrodynamics of self-propulsion near a boundary: Predictions and accuracy of far-field approximations, J. Fluid Mech. **700**, 105 (2012).

[14] Rothschild, Non-random distribution of bull spermatozoa in a drop of sperm suspension, Nature (London) **200**, 381 (1963).
[15] A. P. Berke, L. Turner, H. C. Berg, and E. Lauga, Hydrodynamic attraction of swimming microorganisms by surfaces, Phys. Rev. Lett. **101**, 038102 (2008).
[16] G. Li and J. X. Tang, Accumulation of microswimmers near a surface mediated by collision and rotational Brownian motion, Phys. Rev. Lett. **103**, 078101 (2009).
[17] P. D. Frymier, R. M. Ford, H. C. Berg, and P. T. Cummings, Three-dimensional tracking of motile bacteria near a solid planar surface, Proc. Natl. Acad. Sci. (USA) **92**, 6195 (1995).
[18] E. Lauga, W. R. DiLuzio, G. M. Whitesides, and H. A. Stone, Swimming in circles: Motion of bacteria near solid boundaries, Biophys. J. **90**, 400 (2006).
[19] S. E. Hulme, W. R. DiLuzio, S. S. Shevkoplyas, L. Turner, M. Mayer, H. C. Berg, and G. M. Whitesides, Using ratchets and sorters to fractionate motile cells of *Escherichia coli* by length, Lab Chip **8**, 1888 (2008).
[20] A. Zöttl and H. Stark, Nonlinear dynamics of a microswimmer in Poiseuille flow, Phys. Rev. Lett. **108**, 218104 (2012).
[21] A. Zöttl and H. Stark, Periodic and quasiperiodic motion of an elongated microswimmer in Poiseuille flow, Eur. Phys. J. E **36**, 4 (2013).
[22] L. Zhu, E. Lauga, and L. Brandt, Low-Reynolds-number swimming in a capillary tube, J. Fluid Mech. **726**, 285 (2013).
[23] A. Acemoglu and S. Yesilyurt, Effects of geometric parameters on swimming of micro organisms with single helical flagellum in circular channels, Biophys. J. **106**, 1537 (2014).
[24] M. Binz, A. P. Lee, C. Edwards, and D. V. Nicolau, Motility of bacteria in microfluidic structures, Microelectron. Eng. **87**, 810 (2010).
[25] P. M. Slovak, G. H. Wadhams, and J. P. Armitage, Localization of MreB in *Rhodobacter sphaeroides* under conditions causing changes in cell shape and membrane structure, J. Bacteriol. **187**, 54 (2005).
[26] J. P. Armitage, T. P. Pitta, M. A.-S. Vigeant, H. L. Packer, and R. M. Ford, Transformations in flagellar structure of *Rhodobacter sphaeroides* and possible relationship to changes in swimming speed, J. Bacteriol. **181**, 4825 (1999).
[27] J. J. L. Higdon, The hydrodynamics of flagellar propulsion: Helical waves, J. Fluid Mech. **94**, 331 (1979).
[28] L. Turner, W. S. Ryu, and H. C. Berg, Real-time imaging of fluorescent flagellar filaments, J. Bacteriol. **182**, 2793 (2000).
[29] L. Turner, A. S. Stern, and H. C. Berg, Growth of flagellar filaments of *Escherichia coli* is independent of filament length, J. Bacteriol. **194**, 2437 (2012).
[30] C. Pozrikidis, *Boundary Integral and Singularity Methods for Linearized Viscous Flow* (Cambridge University Press, New York, 1992).
[31] N. Phan-Thien, T. Tran-Cong, and M. Ramia, A boundary-element analysis of flagellar propulsion, J. Fluid Mech. **184**, 533 (1987).
[32] J. B. Keller and S. I. Rubinow, Swimming of flagellated microorganisms, Biophys. J. **16**, 151 (1976).
[33] J. D. Klein, A. R. Clapp, and R. B. Dickinson, Direct measurement of interaction forces between a single bacterium and a flat plate, J. Colloid Interface Sci. **261**, 379 (2003).
[34] T. Goto, T. Nakai, and K. Aoki, Boundary element analysis on transition of distance and attitude of a bacterium near a rigid surface, J. Biomechan. Sci. Eng. **5**, 329 (2010).
[35] H. C. Berg and L. Turner, Chemotaxis of bacteria in glass capillary arrays. *Escherichia coli*, motility, microchannel plate, and light scattering, Biophys. J. **58**, 919 (1990).
[36] J.-M. Swiecicki, O. Sliusarenko, and D. B. Weibel, From swimming to swarming: *Escherichia coli* cell motility in two-dimensions, Integr. Biol. **5**, 1490 (2013).
[37] H. Shum and E. A. Gaffney, The effects of flagellar hook compliance on motility of monotrichous bacteria: A modeling study, Phys. Fluids **24**, 061901 (2012).
[38] P. Ganatos, R. Pfeffer, and S. Weinbaum, A strong interaction theory for the creeping motion of a sphere between plane parallel boundaries. Part 2. Parallel motion, J. Fluid Mech. **99**, 755 (1980).
[39] V. Kantsler, J. Dunkel, M. Polin, and R. E. Goldstein, Ciliary contact interactions dominate surface scattering of swimming eukaryotes, Proc. Natl. Acad. Sci. (USA) **110**, 1187 (2013).